Olduvai domain expression downregulates mitochondrial pathways: implications for human brain evolution and neoteny

Jonathon G. Keeney,[1,*] David Astling,[1] Vanessa Andries,[2,3,#] Karl Vandepoele,[2,3,$] Nathan Anderson,[1] Jonathan M. Davis,[1] Pamela Lopert,[4] Jonathan Vandenbussche,[5,6,&] Kris Gevaert,[5,6] An Staes,[5,6,7] Natasia Paukovich,[1] Beat Vögeli,[1] Kenneth l. Jones,[1] Frans van Roy,[2,3] Manisha Patel,[4] and James M. Sikela[1,,8,^]

[1]Department of Biochemistry and Molecular Genetics, University of Colorado Anschutz Medical Campus, Aurora, CO 80045, USA
[2]Inflammation Research Center, VIB, Ghent, Belgium
[3]Department of Biomedical Molecular Biology, Ghent University, Ghent, Belgium
[4]Department of Pharmaceutical Sciences, School of Pharmacy, University of Colorado Anschutz Medical Campus, Aurora, CO 80045, USA
[5]Department of Biomolecular Medicine, Ghent University, 9052 Ghent, Belgium
[6]VIB Center for Medical Biotechnology, VIB, 9052 Ghent, Belgium
[7]VIB Proteomics Core, 9052 Ghent, Belgium
[8]Human Medical Genetics and Neuroscience Programs, University of Colorado Anschutz Medical Campus, Aurora, CO 80045, USA
*Current address: Department of Biochemistry and Molecular Medicine, George Washington University of Medicine and Health Sciences, Washington, DC 20037, USA
[$]Current address: Department of Clinical Chemistry, Ghent University Hospital, Ghent, Belgium
[#]Current address: Department of Internal Medicine and Pediatrics, Ghent University, Ghent, Belgium
[&]Current address: RIC group, P. Kennedypark 6, 8500 Kortrijk, Belgium
[^]Corresponding author: James M. Sikela, james.sikela@cuanschutz.edu

Abstract

Encoded by the NBPF gene family, Olduvai (formerly DUF1220) protein domains have undergone the largest human lineage-specific copy number expansion of any coding region in the genome. Olduvai copy number shows a linear relationship with several brain size-related measures and cortical neuron number among primates and with normal and disease-associated (micro- and macrocephaly) variation in brain size in human populations. While Olduvai domains have been shown to promote proliferation of neural stem cells, the mechanism underlying such effects has remained unclear. Here, we investigate the function of Olduvai by transcriptome and proteome analyses of cells overexpressing *NBPF1*, a gene encoding 7 Olduvai domains. Our results from both RNAseq and mass spectrometry approaches suggest a potential downregulation of mitochondria. In our proteomics study, a Gene Ontology (GO) enrichment analysis for the downregulated proteins revealed a striking overrepresentation of the biological process related to the mitochondrial electron transport chain (*p* value: 1.81e−11) and identified deregulation of the NADH dehydrogenase activity (*p* value: 2.43e−11) as the primary molecular function. We verify the reduction of apparent mitochondria via live-cell imaging experiments. Given these and previous Olduvai findings, we suggest that the Olduvai-mediated, dosage-dependent reduction in available energy via mitochondrial downregulation may have resulted in a developmental slowdown such that the neurogenic window among primates, and most extremely in humans, was expanded over a greater time interval, allowing for production of greater numbers of neurons and a larger brain. We further suggest that such a slowdown may extend to other developmental processes that also exhibit neotenic features.

Introduction

Olduvai protein domains (formerly DUF1220 [Sikela and van Roy, 2017]) show a major increase in copy number in monkeys, apes, and especially humans, where they have undergone the single greatest human-specific increase in copy number of any protein coding sequence in the genome (Fortna et al., 2004; Popesco et al., 2006). Olduvai domains are encoded almost exclusively by the NBPF gene family (Vandepoele et al., 2005) and can be divided into six clades, three conserved domains (CON1–3), and three human lineage-specific domains (HLS1–3)(O'Bleness et al., 2012), all of which are intrinsically disordered (Issaian et al., 2019; Paukovich et al., 2022). In addition, Olduvai copy number shows a strong linear association with several brain size-related measures and with estimated numbers of cortical neurons in the primate lineage (Dumas et al., 2012; Keeney et al., 2015a; Zimmer and Montgomery, 2015). Within the human lineage, Olduvai copy number variations have been implicated in several neurodevelopmental disorders (macrocephaly, microcephaly, autism, and schizophrenia) and cognitive performance (Dumas et al., 2012; Davis et al., 2015a, 2015b, 2019; Searles Quick et al., 2015). Interestingly, the proproteins encoded by all expanded NBPF genes (that is, featuring more than one HLS Olduvai triplet) are post-translationally cleaved such that the primary functional units in humans are independent Olduvai triplet proteins (Pacheco et al., 2022), suggesting that the target of selection was a dosage increase of Olduvai protein. In addition to showing an association of Olduvai dosage with increased neurogenesis in the primate lineage, we have also shown that these domains can stimulate proliferation in human neural stem cells *in vitro* (Keeney et al., 2015a).

Although these previous findings give us insight into the genomic relevance and large-scale effects of Olduvai expression, investigating its role at the molecular level is imperative for understanding its implications for human health and development. In this study, we use transcriptomics and proteomics to identify pathways in which Olduvai domains may be functioning. Using a colon cancer cell line with low endogenous Olduvai expression (DLD1Tr21) (Vandepoele et al., 2008), we evaluated the effects of inducible forced overexpression of *NBPF1*, a gene encoding 7 Olduvai domains. The results are considered in terms of the relationship between mitochondrial output and neurogenesis and are discussed regarding their potential relevance to (1) primate-specific scaling rules regarding the size and number of brain neurons within the primate order, (2) the extended window of neurogenesis that is found during primate brain development, and (3) the potential impact on neoteny in primate and human evolution.

Methods

Cell culture and live-cell imaging

Doxycyclin hydrochloride (Dox; Sigma, Grand Island, New York) was used at a final concentration of 2 µg/ml to induce expression of either NBPF1-IRES-EGFP or EGFP in DLD1Tr21/NBPF1 and DLD1Tr21/Mock cells, respectively. DLD1Tr21/Mock and DLD1Tr21/NBPF1 cells were described previously (Vandepoele et al., 2008). Briefly, in the colon cancer cell line DLD1Tr21 Tet-On originally obtained from Van de Wetering et al., 2002, a Tet-On system activates transcription of the gene of interest in the presence of Dox. The cDNA for NBPF1-IRES-EGFP, fused to an amino-terminal flag tag, was cloned in the pcDNA4/TO vector (Invitrogen). This construct was stably transfected in DLD1Tr21 cells and subcloned after fluorescence-activated cell sorting. A final clone was more than 90% positive for flag-tagged NBPF1 expression upon induction with Dox for 48 h. For mitochondrial analysis, media was removed at 24 h after plating and replaced with media including 200 nM MitoTracker CMSROX (Gibco) and either 2 µg/ml Dox or no Dox. Cells were then cultured at 37°C in 5% CO_2 in an IncuCyte kinetic life cell imaging system (Essen Bioscience, Ann Arbor, MI). Red (MitoTracker), green (from IRES-EGFP on the construct, indicating successful Dox induction), and phase contrast images were collected every 4 h.

Library preparation and Illumina sequencing

For both DLD1Tr21/NBPF1 and DLD1Tr21/Mock cells, eight T-175 flasks (Falcon) were cultured at 37°C in 5% CO2. After 24 h, media was changed. Four flasks of each cell line were refreshed with medium containing Dox, whereas the medium of the remaining four flasks was refreshed with medium only. After 24 h, cells were trypsinized (Gibco) and collected in complete medium. cDNA libraries were constructed starting from 1 µg total RNA. PolyA-plus mRNAs were selected for by using oligo dT beads according to the manufacturer's instructions, then reverse transcribed to cDNA and prepared for next-generation sequencing according to the manufacturer's protocol (Illumina TruSeq RNA Sample Preparation v2 Guide). The cDNA libraries were validated on the Agilent 2100 Bioanalyzer using DNA-1000 chip. Cluster generation was done on the Illumina cBot using a Single Read Flow Cell with a Single

Read cBot reagent plate (TruSeq SR Cluster Kit). Sequencing of the clustered flow cell was performed on the Illumina HiSeq 2000 using TruSeq SBS v3 reagents. The sequencer was programmed with a single read at 100 cycles. Sequencing images were generated through the sequencing platform (Illumina HiSeq, 2000). The raw data were analyzed in four steps: image analysis, base calling, sequence alignment, and variant analysis and counting. An additional step was required to convert the base call files (.bcl) into *_qseq.txt files. For multiplexed lanes/samples, a de-multiplexing step was performed before the alignment step.

RNAseq data analysis

On average, we obtained 20 million (range = 12–30 million) single-end 100 bp sequencing reads per sample. Reads were mapped against the human genome using Tophat (version 2.0.9) (Kim et al., 2013) and the NCBI reference annotation (build 37.2) as a guide. We allowed 3 mismatches for the initial alignment and 2 mismatches per segment with 25-bp segments. On average, 90% (85%–94%) of the reads aligned to the human genome. Next, we employed Cufflinks (version 2.1.1) (Trapnell et al., 2010) to assemble the transcripts using the RefSeq annotations as the guide but allowing for novel isoform discovery in each sample. Isoforms were ignored if the number of supporting reads was less than 30 and if the isoform fraction was less than 10% for the gene. The data were fragment bias corrected, multi-read corrected, and normalized by the total number of reads. The transcript assemblies for each sample were merged using Cuffmerge (Trapnell et al., 2010). We next computed the transcripts' FPKM values (Fragments Per Kilobase of exon per Million fragments mapped) by rerunning Cufflinks using the merged assembly as the guide. Gene expression was estimated by summing the FPKM values of multiple transcripts that represent the same gene. All other analyses were performed in R/Bioconductor (R version 3.0.1; R Development Core, 2011).

Significantly changed genes were identified using the R package LIMMA (Smyth, 2005). Significant genes were identified using the lmFit, eBayes, and decideTests functions (FDR < 0.05 and fold change > 1.5) from the LIMMA package. The statistics were moderated by LIMMA using empirical Bayes shrinkage (via the eBayes function), global multiple testing strategy, and Benjamini & Hochberg adjustment. Gene set enrichment analysis (GSEA) was conducted using the Kyoto Encyclopedia of Genes and Genomes (KEGG) and Gene Ontology (GO) gene set definitions obtained from the Molecular Signatures Database v.3.1. Enriched pathways were identified by running GSEA using 1,000 permutations as a standalone Java app (version 2.0.13; Subramanian et al., 2007).

Proteomics

Stable isotope labeling by amino acids in cell culture (SILAC) with heavy arginine and lysine was used for mass spectrometry-based quantitative proteomic analysis (Colaert et al., 2010). However, its accuracy is compromised by the metabolic conversion of arginine to proline in eukaryotes. As a result, $^{13}C_6$-Arg gets partly converted into $^{13}C_5$-Pro, which results in the generation of multiple satellite peaks for Pro-containing tryptic peptides in the labeled state. This hampers accurate quantitation. We therefore optimized the $^{13}C_6$-Arg concentration of the DLD1Tr21 medium and determined that 30 mg $^{13}C_6$-Arg per l

medium was optimal to minimize $^{13}C_6$-Arg conversion and that the cells had to be grown for 2 weeks in SILAC medium to obtain full labeling of the cells.

Medium for light labeled cells (− Dox) was RPMI-1640 medium (without Arg and Lys), supplemented with GlutaMax (Gibco), 10% dialyzed fetal calf serum, 0.03 mg/ml $^{12}C_6$-Arg and 0.03 mg/ml $^{12}C_6$-Lys.

Medium for heavy labeled cells (+ Dox) was RPMI-1640 medium (without Arg and Lys), supplemented with GlutaMax, 10% dialyzed fetal calf serum, 0.03 mg/ml $^{13}C_6$-Arg and 0.03 mg/ml $^{13}C_6$-Lys. Dox for the induction of NBPF1 expression was added to the medium at a final concentration of 2 µg/ml.

Cells were grown for two weeks in the appropriate SILAC medium, and cell pellets were then resuspended in 0.5 ml of cell lysis buffer containing 50 mM sodium phosphate pH 7.5, 100 mM NaCl, 0.8% CHAPS (w/v), and Complete Protease Inhibitor cocktail (Roche). Cells were lysed on ice for 30 min, and the insoluble fraction was removed by centrifugation (15 min at 16,000 g at 4°C). Protein measurements of the supernatant occurred by use of the DC Protein Assay kit (Bio-Rad).

The light and heavy labeled samples were mixed in a 1:1 ratio (1.7 mg of protein each). 380 mg guanidinium hydrochloride was added, and the sample volume was adjusted to 1 ml by adding lysis buffer to obtain a final guanidinium hydrochloride concentration of about 4 M.

S-reduction and S-alkylation were performed by adding 26 µl of freshly prepared and pH-adjusted 570-mM TCEP.HCl solution and 40 µl of freshly prepared 750 mM iodoacetamide solution, obtaining a final concentration of 15 mM TCEP.HCl and 30 mM iodoacetamide. The reaction proceeded for 15 min while mixing at 30°C in the dark. The sample was then desalted on a NAP-10 column in 20 mM ammonium bicarbonate pH 7.6. The protein concentration in the NAP-10 eluate was measured using the Bio-Rad DC Protein Assay Kit, and 750 µl (0.868 mg protein) was taken to carry out the next steps. The sample was boiled for 5 min and directly transferred to ice for 10 min. Trypsin was added in a trypsin/protein ratio of 1/50 (w/w), and the sample was incubated overnight at 37°C.

The peptide mixture was dried in a Speedvac and then redissolved in 1% acetic acid. After checking the pH, the sample was loaded on a HPLC column and 1 min fractions were collected between 20 and 80 min. Fractions with a retention time difference of 20 min were pooled, dried down, and analyzed with the LTQ-Orbitrap mass spectrometer. GO analysis was performed with WebGestalt V2 (Zhang et al., 2005) comparing the obtained results to the complete human proteome. The distribution of ratio values (light/heavy) was analyzed using a base 2 logarithmic scale, which is a common practice for protein expression data (MacCoss et al., 2003).

Results

Identification of mitochondria-related pathways by RNAseq of NBPF1-expressing cells

To identify possible pathways in which Olduvai may be functioning, DLD1Tr/21 cells artificially induced to overexpress NBPF1 or a mock construct were evaluated by RNAseq and compared to uninduced cells from the same lineages. GSEA of downregulated genes upon NBPF1 overexpression identified an abundance of pathways related to mitochondrial function with high normalized enrichment score (NES)

and low false discovery rate (FDR) scores, wherein all but one ("proteasome complex") of the pathways identified are related to metabolic function (Table 1). In contrast, none of the pathways in the mock cell line were found to be significantly enriched using an FDR cutoff of 0.05 (Supplemental Table 1). Although several GO terms identified in the list of upregulated pathways found in the DLD1Tr21/NBPF1 line showed relatively low FDR values, no clearly discernible pattern was evident among these (Supplemental Table 2). In the mock cell line, no significant changes were detected (Supplemental Table 3). A GSEA profile also indicates an enrichment of mitochondrially related genes for DLD1Tr21/NBPF1 when compared to DLD1Tr21/Mock, which is more randomly distributed (Figure 1).

Identification of mitochondria-related pathways by proteomics of NBPF1-expressing cells

We hypothesized that investigating proteome differences between DLD1Tr21/NBPF1 cells in the absence of Dox (no NBPF1 expression) compared to the presence of Dox (NBPF1 expression) could provide valuable complementary information to our RNAseq results and could further scrutinize the role of NBPF1. To this end, cells were subjected to stable isotope labeling by amino acids in cell culture (SILAC) for quantitative proteomics (Ong et al., 2002). In the present case, DLD1Tr21/NBPF1 –Dox cell cultures were labeled with light $^{12}C_6$-Lys/Arg amino acids, and the DLD1Tr21/NBPF1 +Dox cell cultures were labeled with heavy $^{13}C_6$-Lys/Arg amino acids. Note that there is hardly any biochemical difference between the heavy and the natural amino acid isotopes, and cells incubated in heavy amino acids are expected to behave exactly like the control cell population grown in the presence of natural amino acids. SILAC labeling is efficient and reproducible as the incorporation of the isotope label is complete (Ong et al., 2002). LC-MS/MS analysis of the mixture of light and heavy peptides allows quantitative assessment of the identified proteins in control versus induced DLD1Tr21/NBPF1 cell cultures.

After growing DLD1Tr21/NBPF1 cell cultures in the appropriate SILAC medium for 2 weeks, we checked NBPF1 expression by immunofluorescence and observed that the DLD1Tr21/NBPF1 cells were indeed expressing NBPF1 and only when Dox was added to the medium (Supplemental Figure 1).

Mass spectrometry resulted in the acquisition of 104,523 MS/MS spectra, which yielded 21,176 unique peptide identifications (Swiss-Prot database, restriction *Homo sapiens*) and 4,008 distinct proteins (Mascot software, 99% confidence). The $\log_2$ light/heavy ratios were tightly distributed around zero, indicating that global protein abundance was not affected by NBPF1 expression. However, a total of 79 proteins showing differential expression were identified at the 99% confidence interval. Of these, 52 proteins were downregulated upon NBPF1 expression (light/heavy ratio > 1) (Supplemental Table 4), whereas 27 proteins were upregulated upon NBPF1 expression (light/heavy ratio < 1) (Supplemental Table 5).

Gene Ontology (GO) enrichment analysis (Zhang et al., 2005) for the upregulated proteins revealed an overrepresentation in amino acid biosynthesis as biological process (adjusted [adj.] *p* value: 7.78e−05) and ribonucleotide binding as molecular function (adj. *p* value: 5.36e−01), although with lower statistical significance. However, GO enrichment analysis for the downregulated proteins revealed a statistically significant overrepresentation in the biological process related to the mitochondrial electron transport

chain (ETC) (adj. *p* value: 1.81e−11) and identified deregulation of the NADH dehydrogenase activity (adj. *p* value: 2.43e−11) as molecular function.

Confirmation of mitochondrial downregulation by live-cell imaging

Red fluorescence measured *in vivo* in both DLD1Tr21/NBPF1 and DLD1Tr21/Mock cell lines stained with MitoTracker CMSROX indicated strong downregulation of genes related to mitochondrial function, in line with our RNAseq and proteomic data. Because the MitoTracker reagent binds directly to the mitochondrial membrane based on the proton gradient, this may indicate either fewer mitochondria or an attenuated proton gradient or changes in the mitochondrial membrane affecting protein content or conformation. Three metrics found to be strongly different are percentage of red coverage (amount of red signal in the viewable area), red intensity (mean red signal intensity across the entire image), and red object count (number of objects meeting the minimum threshold to be called “red”) (Figure 2). Red object confluence starts near 60% in all wells and shows at least a gradual decrease in all wells, but only in the well with NBPF1-overexpressing cells does it show an immediate and permanent drop to near zero, while no other condition approaches zero. For average red intensity, most wells plateau near 24 h around 1.5 x 10^8 relative units, while the NBPF1-overexpressing cells drop to near zero. Similarly, the number of red objects stays relatively constant in the DLD1Tr21/NBPF1 uninduced cell line and even increases in the DLD1Tr21/Mock cell line (induced and uninduced), while the DLD1Tr21/NBPF1 induced cell line immediately drops to very low numbers. When the threshold of detection is set to only detect very bright signals that may be indicative of dividing cells, there is no change between wells (data not shown). When cell density is varied, the drop in MitoTracker signal observed in Figure 1 is not detected at lower cell densities (Supplemental Figures 3–6).

Discussion

Olduvai-mediated mitochondrial downregulation

Here we used a series of experimental approaches to investigate the effects of overexpression of Olduvai protein domains. One of our primary findings is that both RNAseq and proteomic studies of Olduvai/NBPF overexpression identified genes/proteins associated with mitochondria. Specifically, both approaches found Olduvai/NBPF overexpression to be associated with a downregulation of transcripts related to mitochondrial function. For example, 8 of the top 24 downregulated proteins in the proteomic dataset were found in common in the RNAseq data (UQCRC1, PHB, PHB2, IMMT, NDUFS2, NDUFS8, NDUFS1, and UQCRB). All were identified as downregulated upon Olduvai/NBPF overexpression, and all play a role in mitochondrial function. It should be noted that one RNAseq sample showed a particularly strong downregulation of these genes, while the others were more modest, though still significant (Supplemental Figure 2). Why the mass spectrometry data showed a strong downregulation of mitochondria and why it was corroborated by the RNAseq data, but not by all samples, was further investigated. Analysis of EGFP expression level indicated that RNAseq sample 3 also showed a much higher EGFP expression level, indicating stronger output of the exogenous construct, which may explain the result (Supplemental Table 6). It is also known that brain architecture in the primate lineage is unique in that it maintains a near-constant neuronal cell density (Herculano-

Houzel, 2009). Therefore, we explored whether the downregulation of mitochondria was cell-density dependent and found evidence that the effect only occurs at high densities.

These results indicate that overexpression of Olduvai domains leads to a decrease in mitochondrial activity, though whether this result is due to a reduction in total mitochondria or a reduction in the proton gradient is unclear. Interestingly, the functional output of mitochondria in cells with upregulated Olduvai is unexpectedly modest (data not shown), given the striking decrease in MitoTracker signal, which may be consistent with the findings of Diaz-Cuadros et al., (2023). The apparent drop in functional output is particularly weak in light of recent work demonstrating that doxycycline inhibits mitochondrial biogenesis (Scatena et al., 2018) (though we note that it does not affect the apparent red signal as demonstrated by the mock + doxycycline experimental condition). This is in stark contrast to the substantial drop in MitoTracker signal observed in Figure 2. As discussed below, it is conceivable that this incongruence is due to a difference in cell density, as this was the primary difference in methodological setup between these two experiments. When conditions used for Figure 2 were repeated but cell density was varied, the large drop in MitoTracker signal was observed at high cell density (near confluency) but was not observed at lower cell densities (Supplemental Figures 3–6). The reduction in apparent mitochondria may therefore indicate an Olduvai-mediated shift in cellular energetics toward a more restricted mode.

Neuronal cell density

Alternatively, our results may be indicative of an Olduvai-mediated cessation of oxidative phosphorylation, restricting energy availability. This is consistent with the finding in Keeney et al., 2015b, that mice in which the ancestral form of Olduvai was knocked out show hyperactivity. It may also be consistent with a separate investigation of knockin mice, which found embryonic lethality in homozygous mutants and what may be a developmental slowing in gross morphology in these embryos (Keeney, 2014). Such a shift to restrict energy availability may contribute to the primate tendency to maintain neurons at a constant density (Herculano-Houzel, 2009) (implying a relatively small size), rather than decreasing density (implying a scaling up of neuron size), with increasing brain and body mass, as occurs in many other mammals. Indeed, the maintenance of a relatively constant neuron size has been shown to be a hallmark of primate brains and is a phenomenon generally absent among non-primate mammalian brains (Herculano-Houzel, 2009). Olduvai copy number parallels this trend, with primate brain expansion being primarily the result of increasing neuron number while keeping neuron size constant, and may therefore be involved in maintaining cell density.

As Olduvai has previously been associated with increasing numbers of neurons in primates (Dumas et al., 2012), a role for Olduvai in restricting available energy may explain the model of primate brain evolution in which neuronal density is held constant throughout the primate order: by restricting the amount of energy available to each cell—and therefore restricting cell size—more metabolic energy is available to the developing organism. In theory, the effect could be greater numbers of neurons all held at the same size. Brain size and neuron size would in this scenario be fundamentally metabolically driven, with Olduvai domains acting like a molecular switch to divert the metabolic energy one way or the other. This would be consistent with the observation that primates tend to have much slower

metabolisms than would be expected for their body size (Pontzer et al., 2014). It is therefore conceivable that restraining mitochondrial output is having a proliferative effect of its own. It is also possible, however, that this effect is not applicable to the brain, since a non-neural DLD1 cell line was used in our experiments. The comparatively low Olduvai expression in the background colon cancer DLD1 cell line was experimentally important in emphasizing the difference between low Olduvai expression and high Olduvai expression but should be kept in consideration when trying to generalize. It is worth noting, however, that Olduvai is expressed in many tissues (Popesco et al., 2006) and may indeed therefore have a more general function in addition to its involvement in neural function. Still, future work should investigate potential differences in neural cell lines and whether Olduvai is related to the maintenance of cell density and, if so, what the nature of the relationship is.

Brain evolution and neoteny

Perhaps the most intriguing possibility is that the Olduvai-meditated reduction in energy available to cells may be related to neoteny, a specific form of heterochrony in which there is a delay in the timing of a developmental event in one species relative to another. Neoteny can therefore appear as the prolonged retention of infantile or juvenile characteristics in the adult. This differential timing during development can substantially change the size and shape of an organ or organism. More specifically, it is thought to be capable of greatly increasing the size of structures, including the brain (Gould, 1977). Indeed, several recent reports have begun to implicate mitochondria function in the timing of development and the neotenic events that characterize human-specific brain evolution (Namba et al., 2020; Diaz-Cuadros et al., 2023; Iwata et al., 2023; Casimir et al., 2024; Lindhout et al., 2024). For example, it was shown that increasing mitochondrial metabolism accelerates neuronal maturation while decreasing metabolism had the opposite effect. These studies suggest that mitochondria may serve as a species-specific pacemaker of development (Liu and Auwerx, 2023), and the findings we report here fit with this trend. In this regard, it is worth pointing out that our proteomics analysis found that the most significantly altered functional class of genes that were downregulated by Olduvai expression was mitochondrial genes involved in the electron transport chain (ETC) and NADH processes. These are the same two mitochondrial mechanisms that have been implicated in driving species-specific developmental rates (Diaz-Cuadros et al., 2023). Specifically, inhibiting the ETC slowed developmental timing by impacting the NAD/NADH redox balance while, conversely, increasing NADH action accelerated developmental timing.

Given these and previous Olduvai studies, we suggest that the Olduvai-mediated, dosage-dependent reduction in available energy via mitochondrial downregulation may have resulted in a developmental slowdown such that the neurogenic window among primates, and especially in humans, was expanded over a greater time interval, allowing for production of greater numbers of neurons. This prolongation of neural development, and general neoteny, are thought to have increased as one moves from rodent (mouse) to primates and among primates from monkey to ape to human (Kornack and Rakic, 1998; Thiessen, 1997), patterns that are mirrored by Olduvai copy number among these species (O'Bleness et al., 2012). Such a link between Olduvai dosage and a metabolic slowdown is also consistent with the previously mentioned finding that mice lacking Olduvai domains show a pronounced hyperactivity phenotype (Keeney et al., 2015b). In addition to extending the window of progenitor proliferation, an

extended developmental window could give neurons enough time to migrate to their appropriate location in the cortical plate and send out processes before being surpassed by the next wave of post mitotic neurons and thus provide enough time for primate brains to generate many more neurons and neural connections without sacrificing neural structure. Given the pattern of expression reported by Keeney et al., 2015a, one such developmental event that may be impacted is the transition from the first phase of neurodevelopment to the second, as this appears to occur at gestational week (GW) 16 in humans (Nowakowski et al., 2016). A prolonged phase I would be consistent with the pattern of lateral expansion in the neocortex observed in primates and particularly in humans. If Olduvai domains are indeed driving a neoteny phenotype, and given the fact that Olduvai is expressed in many, but not all, tissues, this might help to explain why some, but not all, features of human development appear to be neotenic when compared to other primates.

Pairing of Olduvai and *NOTCH2NL*

The Olduvai findings reported here also have potential relevance to human-specific *NOTCH2NL* genes that have been shown to promote neurogenesis (Fiddes et al., 2018, Suzuki et al., 2018, Florio et al., 2018). The majority of human-specific copies of Olduvai are encoded by three *NBPF* genes that are adjacent to, and tightly co-regulated with, three *NOTCH2NL* genes (Fiddes et al., 2019). These *NBPF/NOTCH2NL* gene pairs evolved jointly, as two-gene units, having recently undergone multiple duplications that added >100 Olduvai copies to the human genome. If the *NOTCH2NL* genes are primarily promoting neural progenitor cell divisions while the Olduvai dosage increase holds the developmental window open longer, it could provide an efficient mechanism for producing more neurons and would provide a compelling explanation for why the Olduvai *NOTCH2NL* pairing has been strongly selected for in recent human evolution.

Finally, it will be interesting to identify the specific molecular agents through which Olduvai is acting to downregulate mitochondrial function and how such a phenomenon is related to the evolutionarily rapid and extreme increase in Olduvai copy number in humans.

Acknowledgments

This work was supported by NIH grants R01 MH081203-01A2 (J.M.S.), R01 MH081203-02S1 (J.M.S.), R01 MH108684 (J.M.S.), and R01 GM150642 (B.V.) and a fellowship from the Coleman Institute for Cognitive Disabilities.

Top 20 GO terms downregulated in DLD1Tr21/NBPF upon RNAseq analysis

	Pathway	Size	NES	FDR
1	MITOCHONDRIAL_INNER_MEMBRANE	54	2.60	0.000
2	MITOCHONDRIAL_MEMBRANE_PART	46	2.57	0.000
3	MITOCHONDRION	245	2.47	0.000
4	ORGANELLE_INNER_MEMBRANE	60	2.46	0.000
5	MITOCHONDRIAL_MEMBRANE	69	2.46	0.000
6	MITOCHONDRIAL_ENVELOPE	75	2.45	0.000
7	MITOCHONDRIAL_PART	94	2.35	0.000
8	PROTON_TRANSPORTING_TWO_SECTOR_ATPASE_COMPLEX	14	2.06	0.007
9	MITOCHONDRIAL_RESPIRATORY_CHAIN	22	2.00	0.012
10	RESPIRATORY_CHAIN_COMPLEX_I	13	1.99	0.013
11	NADH_DEHYDROGENASE_COMPLEX	13	1.98	0.015
12	MITOCHONDRIAL_RESPIRATORY_CHAIN_COMPLEX_I	13	1.96	0.017
13	FATTY_ACID_METABOLIC_PROCESS	31	1.94	0.019
14	MITOCHONDRION_ORGANIZATION_AND_BIOGENESIS	36	1.93	0.020
15	MONOCARBOXYLIC_ACID_METABOLIC_PROCESS	41	1.93	0.019
16	PROTEASOME_COMPLEX	23	1.90	0.026
17	COENZYME_METABOLIC_PROCESS	29	1.88	0.032
18	OXIDOREDUCTASE_ACTIVITY	170	1.85	0.040
19	OXIDOREDUCTASE_ACTIVITY_GO_0016616	34	1.81	0.058
20	HYDROGEN_ION_TRANSMEMBRANE_TRANSPORTER_ACTIVITY	20	1.80	0.062

Table 1. Top-scoring pathways associated with the genes that showed a reduction in expression after exogenous NBPF1 expression

Size: number of genes in the pathway. NES: normalized enrichment score shown as $\log_2$ values; the number of genes detected in our dataset, normalized to the size of the pathway. FDR: false discovery rate.

A

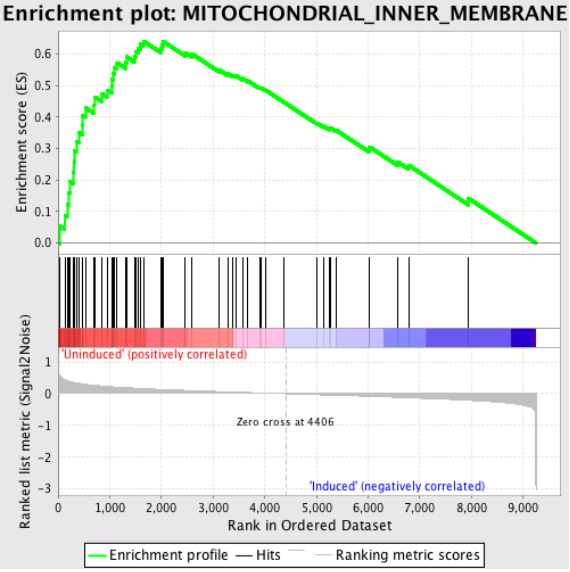

B

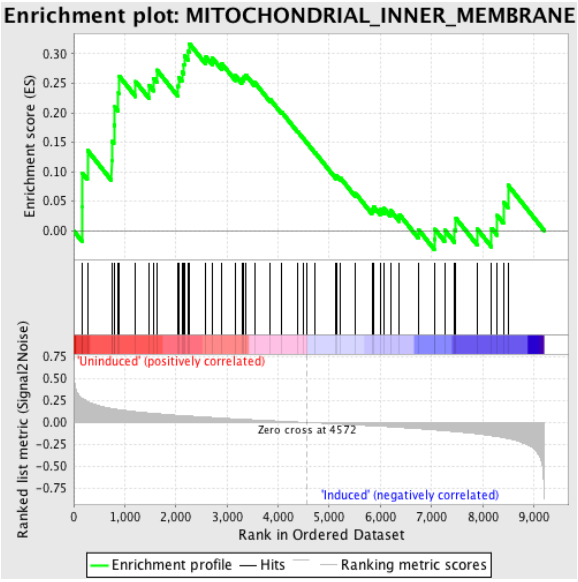

Figure 1. GSEA enrichment profiles of the mitochondrial inner membrane GO gene set

(A) DLD1Tr21/NBPF (B) DLD1Tr21/Mock. The top portion of the plot is the running enrichment score (ES) versus the rank in the ordered gene list. The maximum value at the peak is the ES of the gene set. Note that the ES for the mock cell line is about half that of the NBPF1-induced cells. The middle portion of the plot indicates the position of the members of the gene list within the full rank-ordered gene list. Note that, in (A), the ranking of the genes is weighted more toward the left portion of the plot, whereas in (B), the genes appear more randomly distributed. The bottom portion of the plot shows the signal-to-noise ratio versus gene rank. A positive value indicates correlation with the uninduced samples.

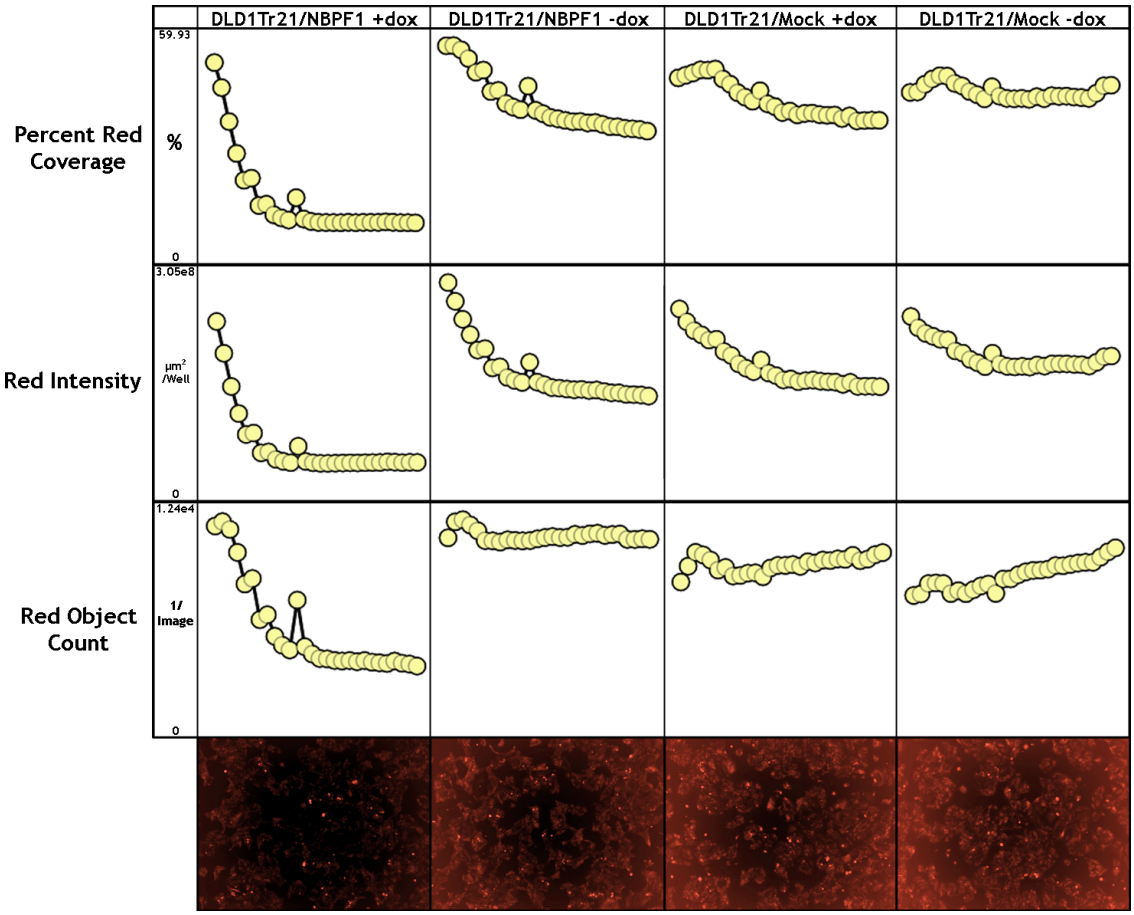

Figure 2. DLD1-NBPF1 or DLD1-MOCK cells incubated with MitoTracker, a reagent that binds to mitochondria and fluoresces red

Each circle represents a time point at 4 h. Red coverage (confluency), average red object intensity, and red object count are plotted against time over the course of 4 days from the time of doxycycline application for each cell line with and without doxycycline to initiate transcription of the transgene. A low magnification example image from each condition is shown below the plots to indicate general levels of red signal.

References

Casimir P, Iwata R, Vanderhaeghen P (2024) Linking mitochondria metabolism, developmental timing, and human brain evolution. Curr Opin Genet Dev 86. https://doi.org/10.1016/j.gde.2024.102182.

Colaert N, Helsens K, Impens F, et al. (2010) Rover: A tool to visualize and validate quantitative proteomics data from different sources. Proteomics 10. https://doi.org/10.1002/pmic.200900379.

Davis JM, Heft I, Scherer SW, Sikela JM (2019) A third linear association between Olduvai (DUF1220) copy number and severity of the classic symptoms of inherited autism. American Journal of Psychiatry 176. https://doi.org/10.1176/appi.ajp.2018.18080993.

Davis JM, Searles Quick VB, Sikela JM (2015a) Replicated linear association between DUF1220 copy number and severity of social impairment in autism. Hum Genet 134. https://doi.org/10.1007/s00439-015-1537-6.

Davis JM, Searles VB, Anderson N, et al. (2015b) DUF1220 copy number is linearly associated with increased cognitive function as measured by total IQ and mathematical aptitude scores. Hum Genet 134:67–75. https://doi.org/10.1007/s00439-014-1489-2.

Diaz-Cuadros M, Miettinen TP, Skinner OS, et al. (2023) Metabolic regulation of species-specific developmental rates. Nature 613. https://doi.org/10.1038/s41586-022-05574-4.

Dumas LJ, O'bleness MS, Davis JM, et al. (2012) DUF1220-domain copy number implicated in human brain-size pathology and evolution. Am J Hum Genet 91. https://doi.org/10.1016/j.ajhg.2012.07.016.

Fiddes IT, Lodewijk GA, Mooring M, et al. (2018) Human-specific NOTCH2NL genes affect notch signaling and cortical neurogenesis. Cell 173. https://doi: 10.1016/j.cell.2018.03.051.

Fiddes IT, Pollen AA, Davis JM, Sikela JM (2019) Paired involvement of human-specific Olduvai domains and NOTCH2NL genes in human brain evolution. Human Genetics 138. https://doi: 10.1007/s00439-019-02018-4.

Florio M, Heide M, Pinson A, et al. (2018) Evolution and cell-type specificity of human-specific genes preferentially expressed in progenitors of fetal neocortex. eLife 7:e32332. http://doi.org/10.7554/eLife.32332.

Fortna A, Kim Y, MacLaren E, et al. (2004) Lineage-specific gene duplication and loss in human and great ape evolution. PLoS Biol 2. https://doi.org/10.1371/journal.pbio.0020207.

Herculano-Houzel S (2009) The human brain in numbers: A linearly scaled-up primate brain. Front Hum Neurosci 3. https://doi.org/10.3389/neuro.09.031.2009.

Issaian A, Schmitt L, Born A, et al. (2019) Solution NMR backbone assignment reveals interaction-free tumbling of human lineage-specific Olduvai protein domains. Biomol NMR Assign 13. https://doi.org/10.1007/s12104-019-09902-0.

Iwata R, Casimir P, Erkol E, et al. (2023) Mitochondria metabolism sets the species-specific tempo of neuronal development. Science 379. https://doi.org/10.1126/science.abn4705.

Keeney, J.G. (2014) Functional investigations of DUF1220 protein domains. Ph.D. diss., University of Colorado Denver, Anschutz Medical Campus,

Keeney JG, Davis JM, Siegenthaler J, et al. (2015a) DUF1220 protein domains drive proliferation in human neural stem cells and are associated with increased cortical volume in anthropoid primates. Brain Struct Funct 220. https://doi.org/10.1007/s00429-014-0814-9.

Keeney JG, O'Bleness MS, Anderson N, et al. (2015b) Generation of Mice Lacking DUF1220 Protein Domains: Effects on Fecundity and Hyperactivity. Mammalian Genome 26. https://doi.org/10.1007/s00335-014-9545-8.

Kim D, Pertea G, Trapnell C, et al. (2013) TopHat2: Accurate alignment of transcriptomes in the presence of insertions, deletions and gene fusions. Genome Biol 14. https://doi.org/10.1186/gb-2013-14-4-r36.

Kornack DR, Rakic P (1998) Changes in cell-cycle kinetics during the development and evolution of primate neocortex. Proc Natl Acad Sci U S A 95. https://doi.org/10.1073/pnas.95.3.1242.

Lindhout FW, Krienen FM, Pollard KS, Lancaster MA (2024) A molecular and cellular perspective on human brain evolution and tempo. Nature 630. http://doi: 10.12688/f1000research.13586.2. eCollection 2017

Liu YJ, Auwerx J (2023) Mitochondria: A "pacemaker" for species-specific development. Mol Cell 83. https://doi.org/10.1016/j.molcel.2023.02.025.

MacCoss MJ, Wu CC, Liu H, et al. (2003) A Correlation Algorithm for the Automated Quantitative Analysis of Shotgun Proteomics Data. Anal Chem 75. https://doi.org/10.1021/ac034790h.

Namba T, Dóczi J, Pinson A, et al. (2020) Human-Specific ARHGAP11B Acts in Mitochondria to Expand Neocortical Progenitors by Glutaminolysis. Neuron 105. https://doi.org/10.1016/j.neuron.2019.11.027.

Nowakowski TJ, Pollen AA, Sandoval-Espinosa C, Kriegstein AR (2016) Transformation of the Radial Glia Scaffold Demarcates Two Stages of Human Cerebral Cortex Development. Neuron 91. https://doi.org/10.1016/j.neuron.2016.09.005.

O'Bleness MS, Michael Dickens C, Dumas LJ, et al. (2012) Evolutionary history and genome organization of duf1220 protein domains. G3: Genes, Genomes, Genetics 2. https://doi.org/10.1534/g3.112.003061.

Ong SE, Blagoev B, Kratchmarova I, et al. (2002) Stable isotope labeling by amino acids in cell culture, SILAC, as a simple and accurate approach to expression proteomics. Mol Cell Proteomics 1. https://doi.org/10.1074/mcp.M200025-MCP200.

Pacheco A, Issaian A, Davis J, et al. (2022) Proteolytic activation of human-specific Olduvai domains by the furin protease. Int J Biol Macromol. http://doi:10.1016/j.ijbiomac.2022.12.260.

Paukovich N, Henen MA, Hussain A, et al. (2022) Solution NMR backbone assignments of disordered Olduvai protein domain CON1 employing Hα-detected experiments. Biomol NMR Assign. https://doi.org/10.1007/s12104-022-10068-5.

Pontzer H, Raichlen DA, Gordon AD, et al. (2014) Primate energy expenditure and life history. Proc Natl Acad Sci U S A 111. https://doi.org/10.1073/pnas.1316940111.

Popesco MC, MacLaren EJ, Hopkins J, et al. (2006) Human lineage-specific amplification, selection, and neuronal expression of DUF1220 domains. Science 313. https://doi.org/10.1126/science.1127980.

R Development Core T (2011) R: A Language and Environment for Statistical Computing. Vienna, Austria : the R Foundation for Statistical Computing. ISBN: 3-900051-07-0. PhD Proposal 1.

Scatena C, Roncella M, Di Paolo A, et al. (2018) Doxycycline, an inhibitor of mitochondrial biogenesis, effectively reduces cancer stem cells (CSCs) in early breast cancer patients: A clinical pilot study. Front Oncol 8. https://doi.org/10.3389/fonc.2018.00452.

Searles Quick VB, Davis JM, Olincy A, Sikela JM (2015) DUF1220 copy number is associated with schizophrenia risk and severity: Implications for understanding autism and schizophrenia as related diseases. Transl Psychiatry 5. https://doi.org/10.1038/tp.2015.192.

Sikela JM, van Roy F (2017) Changing the name of the NBPF/DUF1220 domain to the Olduvai domain. F1000Res 6. https://doi: 10.12688/f1000research.13586.2.

S.J. Gould (1977) Ontogeny and phylogeny. Belknap Press of Harvard University Press, Cambridge, MA.

Smyth GK (2005) Limma: linear models for microarray data BT - Bioinformatics and Computational Biology Solutions Using R and Bioconductor. In: Bioinformatics and Computational Biology Solutions Using R and Bioconductor.

Subramanian A, Kuehn H, Gould J, et al. (2007) GSEA-P: A desktop application for gene set enrichment analysis. Bioinformatics 23. https://doi.org/10.1093/bioinformatics/btm369.

Suzuki IK, Gacquer D, Van Heurck R, et al. (2018) Human-specific NOTCH2NL genes expand cortical neurogenesis through delta/notch regulation. Cell 173. https://doi: 10.1016/j.cell.2018.03.067.

Thiessen D (1997) Bittersweet destiny: The stormy evolution of human behavior. Transaction Publishers. New Brunswick, New Jersey.

Trapnell C, Williams BA, Pertea G, et al. (2010) Transcript assembly and quantification by RNA-Seq reveals unannotated transcripts and isoform switching during cell differentiation. Nat Biotechnol 28. https://doi.org/10.1038/nbt.1621.

Vandepoele K, Andries V, Van Roy N, et al. (2008) A constitutional translocation t(1;17)(p36.2;q11.2) in a neuroblastoma patient disrupts the human NBPF1 and ACCN1 genes. PLoS One 3. https://doi.org/10.1371/journal.pone.0002207.

Vandepoele K, Van Roy N, Staes K, et al. (2005) A novel gene family NBPF: Intricate structure generated by gene duplications during primate evolution. Mol Biol Evol 22. https://doi.org/10.1093/molbev/msi222.

Zhang B, Kirov S, Snoddy J (2005) WebGestalt: An integrated system for exploring gene sets in various biological contexts. Nucleic Acids Res 33. https://doi.org/10.1093/nar/gki475.

Zimmer F, Montgomery SH (2015) Phylogenetic analysis supports a link between DUF1220 domain number and primate brain expansion. Genome Biol Evol 7. https://doi.org/10.1093/gbe/evv122.